

HIGH-RESOLUTION RADIO IMAGING OF GRAVITATIONAL LENSING CANDIDATES IN THE 1 JANSKY BL LAC SAMPLE

TRAVIS A. RECTOR

National Radio Astronomy Observatory, P.O. Box O, Socorro, NM 87801

AND

JOHN T. STOCKE

Center for Astrophysics and Space Astronomy, University of Colorado, Boulder, CO 80309-0389

To appear in AJ.

ABSTRACT

While BL Lacertae objects are widely believed to be highly beamed, low-luminosity radio galaxies, many radio-selected BL Lacs have extended radio power levels and optical emission lines that are too luminous to be low-luminosity radio galaxies. Also, Stocke & Rector discovered an excess of MgII absorption systems along BL Lac sightlines compared to quasars, suggesting that gravitational lensing may be another means of creating the BL Lac phenomenon in some cases. We present a search for gravitationally-lensed BL Lacs with deep, high-resolution, two-frequency VLA radio maps of seven lensing candidates from the 1 Jansky BL Lac sample. We find that none of these objects are resolved into an Einstein ring like B 0218+357, nor do any show multiple images of the core. All of the lensing candidates that were resolved show a flat-spectrum core and very unusual, steep-spectrum extended morphology that is incompatible with a multiply lensed system. Thus, while these observations do not rule out microlensing, no macrolensing is observed.

Subject headings: BL Lacertae Objects — AGN — Gravitational Lenses

1. INTRODUCTION

BL Lacertae objects are an extreme type of Active Galactic Nuclei (AGN), whose hallmark is their “featureless” optical spectra (rest frame $W_\lambda \leq 5\text{\AA}$ for any emission lines present). They are a member of the blazar class of AGN. And like other blazars, their observed properties are thought to due to bulk relativistic outflows. It is believed that most BL Lacs are low-luminosity, Fanaroff & Riley (1974) class 1 radio galaxies (FR–1s) whose jet axes are oriented roughly towards the observer (Blandford & Rees 1978). Several pieces of evidence support this hypothesis; e.g., most BL Lacs have giant elliptical host galaxies in rich galaxy regions (Wurtz et al. 1997) consistent with FR–1 hosts, and most have a highly core-dominated radio structure that is consistent with a beamed source (Antonucci & Ulvestad 1985; Perlman & Stocke 1994; Urry & Padovani 1995). However, there is substantial evidence that not all BL Lacs follow this simple picture, especially within the radio-selected “1 Jansky” (1Jy) sample of BL Lacs (Rector & Stocke 2001; Stickel et al. 1991). In fact, the extended radio power levels for fully one-half of the BL Lacs in the 1Jy sample are too luminous to be FR–1s. These objects also have broad, moderately luminous optical emission lines ($\log L = 41 - 43 \text{ erg s}^{-1}$), which are typically seen in FR–2s but not in FR–1s. Why FR–2-like sources appear in abundance in the 1Jy BL Lac sample but not in X-ray selected samples (Rector et al. 2000) is as yet unknown, although Rector & Stocke (2001) discuss several possible factors.

One of these factors might be gravitational lensing. Stocke & Rector (1997) find an excess of MgII systems along the sightlines of 1Jy BL Lacs. Ten absorption systems were found in the spectra of 37 BL Lacs; and

five of them are very strong ($W_\lambda \geq 1\text{\AA}$), which is four to five times greater than the number expected based upon quasar sightlines, i.e., 2.5 to 3σ greater than the expectation value from Steidel & Sargent (1992). This excess suggests a correlation between the presence of absorbing gas along the BL Lac sightline and the relatively featureless spectra of BL Lac objects, as compared to quasars. Such a correlation can be caused by gravitational microlensing of an AGN by stars associated with the absorbing gas, presumably within an intervening foreground galaxy. Ostriker & Vietri (1990) postulated that BL Lacs may simply be microlensed quasars. In their model, a background quasar is microlensed by stars within a foreground giant elliptical galaxy. The microlensing preferentially amplifies the compact nonthermal continuum over the extended emission lines regions, reducing the observed W_λ of the emission lines. If its continuum is sufficiently boosted by microlensing, a quasar may appear to be a BL Lac object. While it is now clear that the Ostriker & Vietri (1990) model does not explain all BL Lac objects, it may explain some. And indeed, evidence of lensing exists for several BL Lacs, e.g., AO 0235+164 (Stickel, Fried & Kühr 1988; Webb et al. 2000), MS 0205.7+3509 (Stocke, Wurtz & Perlman 1995), PKS 0537–441 (Romero, Surpi & Vucetich 1995), PKS 1413+135 (Perlman et al. 1996), RGB 1745+398 (Nilsson et al. 1999) and three other BL Lacs in an *HST* snapshot survey of BL Lacs (Scarpa et al. 1999). There is also evidence against the lensing hypothesis for some of these objects, e.g., PKS 0537–441 (Falomo, Melnick & Tanzi 1992) and MS 0205.7+3509 (Falomo et al. 1997). Further, Narayan & Schneider (1990) discuss several of these sources in a microlensing context where the foreground galaxy has a gravitational potential too shallow to produce multiple images via macrolensing. Thus it is not known how many BL

Lacs are lensed, nor how many AGN are classified as BL Lacs as a result of lensing.

Unfortunately, it is difficult to test for microlensing on a case-by-case basis. An intervening MgII absorption system is suggestive, but not conclusive, of lensing. Similarly, optical imaging can, and occasionally does, discover an intervening foreground galaxy which is offset from the BL Lac nucleus, e.g., Heidt et al. (1998); although this too is not conclusive evidence. Further, the characteristic light curve of a single microlensing event is likely to be blended into multiple events, thereby producing a variability signature which is not easily differentiated from an intrinsically variable source, e.g. Takalo et al. (1998); although achromatic variability is a lensing characteristic which may be used to differentiate (Webb et al. 2000). While it is not conclusive evidence of microlensing, the detection of macrolensing (i.e., multiple images) remains the only means to confirm that an object is indeed gravitationally lensed. So, despite the suggestive evidence alone, currently there is only one confirmed case of a lensed BL Lac: the “smallest Einstein ring” source B 0218+357. The ring is very compact; it is unresolved at arcsecond-scale resolutions, but is clearly resolved with the VLA A-array at 8.4 GHz and higher frequencies (O’Dea et al. 1992). This compact radio structure is typical of gravitational lenses; e.g., all the lenses currently known in the Jodrell Bank-VLA astronomical survey have angular separations on the order of a few arcseconds or less (King et al. 1997).

Here we present a sensitive, high-resolution imaging study of all of the gravitational lens candidates in the 1Jy BL Lac sample which can be reached by the VLA ($\delta > -20^\circ$). Nearly all of the BL Lacs in the 1Jy sample have now been mapped at high sensitivity with the VLA A-array at 1.4 GHz (Cassaro et al. 1999; Murphy, Browne & Perley 1993; Perlman & Stocke 1994; Rector & Stocke 2001). Based upon these maps lensing candidates were chosen with the following criteria. First, sources were chosen that have an unusual radio morphology which is suggestive of lensing, i.e., very distorted and very luminous extended radio structure. The BL Lacs S4 0814+425 (Murphy, Browne & Perley 1993) and PKS 2131-021 (Rector & Stocke 2001) are examples of objects with compact ($\leq 10''$) radio structure that, if interpreted as classical “triple” sources, appear to have edge-brightened, FR-2 like lobes but with a compact, wide-angle tail morphology that is very unusual for FR-2s. Alternatively, the morphology of both sources could be explained as Einstein rings that are marginally resolved. Secondly, sources were chosen that are unresolved or marginally resolved (i.e., highly core dominated). Thirdly, we chose objects whose optical spectrum contains a strong MgII absorption system. This latter criterion selects only high-redshift objects because only MgII absorption systems with redshifts $z \gtrsim 0.4$ can be detected at optical wavelengths. Naturally, B 0218+357 was excluded from the sample since it has already been established to be a lensed system. Seven other objects from the 1Jy BL Lac sample meet one or more of these criteria and were observed in this study (see Table 1). The columns are: [1] the object name; [2-3] the emission and absorption line redshifts; [4] the 20cm extended radio power (in W Hz^{-1}); and [5] the 20cm radio core

dominance, $f \equiv P_{\text{core}}/P_{\text{ext}}$. Values were obtained from Rector & Stocke (2001) and references within.

2. OBSERVATION AND REDUCTION

We chose to observe with the A-array with a 50 MHz bandwidth to maximize resolution while maintaining good sensitivity to extended, steep-spectrum structure. Each object was observed at two frequencies so that spectral-index maps could be generated. Spectral index maps will show whether an object is a typical core-jet source, in which case the steep-spectrum jets and lobes will be easily differentiated from the flat-spectrum core, or if it is a lensed object with multiple images with the same spectral index. Although not attempted here, polarization-sensitive observations can provide an additional test, as the polarization vectors of a lensed image should be unaffected by the gravitational field of the lens (Dyer & Shaver 1992). Thus, the lensed images of each source component should also have the same polarization percentage and position angle, once corrected for Faraday rotation due to the different light paths. One caveat for both spectral-index and polarization measurements is that BL Lacs are known to vary both quantities on timescales as short as days. Thus, in principle multiple images of an object could display different spectral indices and polarizations due to the difference in light travel times if the variability is intrinsic and not due to the lens.

Lensing candidates that are resolved at 1.4 GHz and have a largest angular size greater than $5''$ were observed at 4.86 GHz (C-band) and 8.46 GHz (X-band) to resolve individual components while maintaining excellent sensitivity to faint extended structure. Smaller sources were observed at 8.46 GHz and 14.94 GHz (U-band) to improve the likelihood of resolving discrete components. The resolution of these maps are ten times greater than maps previously available for these sources.

The seven lensing candidates from the 1Jy BL Lac sample were observed with the VLA A-array on 20 September 1999 and 24 September 1999. Four or five scans of 4–8 minute durations were made for each source at each frequency. Scans were spaced to optimize coverage in the (u, v) plane. The resulting maps have sensitivities of roughly 0.1 to 1 mJy beam $^{-1}$.

Epoch 1995.2 VLA values were used to flux calibrate the maps using multiple observations of 3C 286. Since these sources are highly core-dominated, a point source model was assumed to start the self-calibration process. Phase-only self-calibration in decreasing solution time intervals was used for the first four iterations. Amplitude and phase self-calibration were then used until the maximum dynamic range was achieved, usually requiring only one or two more iterations. The AIPS task IMAGR was used to generate the maps and clean components. Robust weighting (ROBUST = 0.5) was used to achieve a smaller beam FWHM with only a 10–12% increase in noise over natural weighting; see Briggs (1995) for an explanation. The core flux densities were measured by fitting the core with a single Gaussian with the synthesized beam’s parameters. The extended flux was determined by measuring the total flux density with a box enclosing the entire source and then subtracting the core flux density. Throughout this paper we assume $S \propto \nu^{+\alpha}$.

In addition to the radio observations described above,

Hubble Space Telescope and ground-based optical data in the literature (Pursimo et al. 2002; Scarpa et al. 2000) were searched for optical counterparts to bright spots in the radio structure. However, no counterparts to the structure observed in the resolved sources were detected. If these are indeed lensed sources, optical counterparts should be present and be sufficiently bright to distort the observed optical radial profiles of these sources. However, in all cases the objects are unresolved at optical wavelengths.

2.1. Summary of Radio Properties

The VLA continuum and spectral index maps are shown in Figures 1 through 8. A summary of the radio properties is given in Table 2. The columns are: [1] the object name; [2–3] the 4.86 GHz VLA core and extended flux densities (mJy); [4–5] the 8.46 GHz VLA core and extended flux densities (mJy); and [6–7] the 14.94 GHz VLA core and extended flux densities (mJy). The error estimates for extended flux densities are based upon the solid angular extent of the source. For unresolved sources, an upper limit on extended flux is conservatively estimated to be 10σ because faint extended flux may be spreaded over many beams.

2.2. Discussion of Individual Sources

S5 0454+844: This object is unresolved in 8.46 GHz and 14.94 GHz maps to the 0.1 and 0.4 mJy beam⁻¹ level respectively. It is also unresolved in a 1.4 GHz, A-array map to the 0.1 mJy beam⁻¹ (Rector & Stocke 2001). The unresolved nature of this source is not unexpected due to a redshift lower limit of $z = 1.340$ that is based upon a MgII absorption system (Stocke & Rector 1997).

PKS 0735+178: This object has a intervening absorption system at $z = 0.424$ (Carswell et al. 1974; Rector & Stocke 2001). The 8.46 GHz and spectral index maps are overlaid in Figure 1. The 14.94 GHz map is shown in Figure 2. The 8.46 GHz map shows an unusual jet-like morphology to the south and west. The spectral index map confirms that PKS 0735+178 consists of a flat-spectrum core ($\alpha_{14.94}^{8.46} = -0.24$) and steep-spectrum ($\alpha_{14.94}^{8.46} \lesssim -1$) jets, not multiple images of the core.

S4 0814+425: The 1.4 GHz map of this object in Murphy, Browne & Perley (1993) is highly suggestive of a lensed system, with possible multiple images of the core to the northeast and northwest. However, 4.86 GHz and 8.46 GHz maps of this object (Figure 3 and Figure 4) show a jet which originates north of the core and arcs to the northeastern lobe. The spectral index map (Figure 3) confirms that the source consists of a flat-spectrum core ($\alpha_{8.46}^{4.86} = +0.1$) and steep-spectrum ($\alpha_{8.46}^{4.86} \lesssim -1$) jets. The morphology of this source is very unusual; however projection effects may be causing an intrinsically straight jet appear to bend dramatically.

PKS 0823+033: This object is unresolved in both the 8.46 GHz and 14.94 GHz maps to the 0.3 and 0.8 mJy beam⁻¹ level respectively. The object is also unresolved in the 1.4 GHz, A-array map in Murphy, Browne & Perley (1993).

PKS 1749+096: This object is unresolved in both the 8.46 GHz and 14.94 GHz maps to the 0.8 and 0.9 mJy beam⁻¹ level respectively. It is also unresolved in a 1.4 GHz, A-array map to the 0.1 mJy beam⁻¹

(Rector & Stocke 2001). The modest tentative redshift ($z = 0.320$) and the fact that the host galaxy is easily observable (Wurtz et al. 1997) make its very high radio core dominance very unusual. However, the observational limits allow that this source could be a typical FR–1 with a somewhat lower extended radio power level ($\log P_{20\text{cm}} \lesssim 24.5 \text{ W Hz}^{-1}$).

S4 1749+701: This object was slightly resolved in 1.4 GHz map (Rector & Stocke 2001). The 8.46 GHz map (Figure 5) shows a halo morphology around the core with a jet-like extension to the southwest. The halo is mostly resolved out of the 14.94 GHz map (Figure 6) however the extension to the southwest is still visible. The spectral index map (Figure 5) shows a flat-spectrum core ($\alpha_{14.94}^{8.46} = -0.2$) and steep-spectrum ($\alpha_{14.94}^{8.46} \lesssim -1$) halo, indicating that this halo is not an Einstein ring image of the core.

PKS 2131–021: The 1.4 GHz map of this object in Rector & Stocke (2001) is highly suggestive of a lensed system, with possible multiple images of the core to the east and southeast. However, 4.86 GHz and 8.46 GHz maps of this object (Figures 7 and 8) show a very interesting morphology, with a jet that originates to the south-southeast of the core. The jet appears to be significantly distorted and may be helical. There also appears to be lobes roughly 5'' to the east and southeast of the core. It is not clear how these jets propagate to the lobes, although projection effects may cause a single lobe to appear as the two seen. But significant bending is still required, even with the severe projection effects expected in BL Lacs, to cause both lobes to appear on the same side of the core. The spectral index map (Figure 7) shows no evidence of multiple images of the core; and the jet and lobes have indices ($\alpha_{8.46}^{4.86} \lesssim -1$) much steeper than the core ($\alpha_{8.46}^{4.86} = +0.06$). A MERLIN+EVN map of this object shows a jet component 50 mas east-southeast from the core, and multiple components extending to the south out to 350 mas from the core, suggesting a helical motion (Cassaro et al. 2002).

3. DISCUSSION AND CONCLUSIONS

We have presented high-resolution radio continuum and spectral index maps for seven gravitational lensing candidates from the 1Jy BL Lac sample. All of the resolved sources show a flat-spectrum core and steep-spectrum extended radio morphology, as expected for core-jet sources. We note that S4 0814+425 and PKS 2131–021 have very similar, and very unusual, radio morphologies in that both appear to have radio lobes on the same side of the core. This could be caused by an intrinsically bent source seen close to the line of sight, although the required geometry would be rare. If so, these sources should have very high apparent luminosities. This is certainly the case for PKS 2131–021, which has the highest core and extended radio powers of any BL Lac object in the 1Jy sample, discounting uncertain values (Rector & Stocke 2001). The redshift for S4 0814+425 is currently unknown, although it must be $z \geq 0.5$ because it is unresolved at optical wavelengths (Pursimo et al. 2002; Urry et al. 1999); thus it too must have a high apparent radio luminosity. VLBI maps of these sources indicate they are highly core-dominated, supporting the hypothesis they are highly beamed (Cassaro et al. 2002; Gabuzda, Pushkarev & Cawthorne 2000). Unfor-

tunately, further comparison is impossible without a firm redshift for S4 0814+425.

None of the maps show evidence of an Einstein ring or multiply-imaged components; however it is important to note that a foreground galaxy may not cause macrolensing if it has a low surface mass density (Narayan & Schneider 1990). Thus, it is possible that a foreground galaxy may cause significant microlensing, brightening the continuum relative to the emission-line regions, without associated macrolensing. The converse

is also true (Abraham et al. 1993). Thus, these observations do not rule out the possibility of lensing; but they argue strongly against macrolensing. The resolved sources show highly distorted jets and misaligned lobes. These unusual morphologies support the hypothesis that these BL Lacs are highly beamed sources, with radio morphologies that are highly distorted due to projection effects.

REFERENCES

- Abraham, R.G., Crawford, C.S., Merrifield, M.R., Hutchings, J.B. & McHardy, I.M. 1993 ApJ 415, 101.
- Antonucci, R.R.J. & Ulvestad, J.S. 1985 ApJ 294, 158.
- Blandford, R. & Rees, M.J. 1978 in Proc. Pittsburgh Conference on BL Lac Objects, ed. A.N. Wolfe, p. 328.
- Briggs, D. 1995, PhD dissertation, New Mexico Institute of Mining and Technology.
- Carswell, R.F., Strittmatter, P.A., Williams, R.E., Kinman, T.D. & Serkowski, K. 1974 ApJ 190, L101.
- Cassaro, P., Stanghellini, C., Bondi, M., Dallacasa, D., della Ceca, R. & Zappalà, R.A. 1999 A&AS 139, 601.
- Cassaro, P., Stanghellini, C., Dallacasa, D., Bondi, M. & Zappalà, R.A. 2002 A&A 381, 378.
- Dyer, C.C. & Shaver, E.G. 1992 ApJ 390, L5.
- Falomo, R., Melnick, J. & Tanzi, E.G. 1992 A&A 255L, 17.
- Falomo, R., Kotilainen, J., Pursimo, T., Sillanpää, A., Takalo, L. & Heidt, J. 1997 A&A 321, 374.
- Fanaroff, B.L. & Riley, J.M. 1974 MNRAS 167, 31.
- Gabuzda, D.C., Pushkarev, A.B. & Cawthorne, T.V. 2000 MNRAS 319, 1109.
- Heidt, J. et al. 1998, in Proc. Turku Conference on BL Lac Phenomenon, ed. L. Takalo.
- King, L.J. et al. 1997 MNRAS 289, 450.
- Murphy, D.W., Browne, I.W.A. & Perley, R.A. 1993 MNRAS 264, 298.
- Nilsson, K., Takalo, L.O., Pursimo, T., Sillanpää, A., Heidt, J., Wagner, S.J., Laurent-Muehleisen, S.A. & Brinkmann, W. A&A 343, 81.
- Narayan, R. & Schneider, P. 1990 MNRAS 243, 192.
- O'Dea, C.P. et al. 1992 AJ 104, 1320.
- Ostriker, J.P. & Vietri, M. 1990 Nature 344, 45.
- Padovani, P. & Urry, C.M. 1990 ApJ 356, 75.
- Padovani, P. & Giommi, P. 1995 ApJ 444, 567.
- Perlman, E.S. & Stocke, J.T. 1994 AJ 108, 56.
- Perlman, E.S., Carilli, C.L., Stocke, J.T. & Conway, J. 1996 AJ 111, 1839.
- Pursimo, T., Nilsson, K., Takalo, L.O., Sillanpää, A., Heidt, J. & Pietilä, H. 2002 A&A 381, 810.
- Rector, T.A., Stocke, J.T., Perlman, E.S., Morris, S.L. & Gioia, I.M. 2000 AJ 120, 1626.
- Rector, T.A. & Stocke, J.T. 2001 AJ 122, 565.
- Romero, G.E., Surpi, G. & Vucetich, H. 1995 A&A 301, 64.
- Scarpa, R., Urry, C.M., Falomo, R., Pesce, J.E., Webster, R., O'Dowd, M. & Treves, A. 1999 ApJ 521, 134.
- Scarpa, R., Urry, C.M., Falomo, R., Pesce, J.E. & Treves, A. 2000 ApJ 532, 740.
- Steidel, C.C. & Sargent, W.L.W. 1992 ApJS 80, 90.
- Stocke, J.T., Wurtz, R.E. & Perlman, E.S. 1995 ApJ 454, 55.
- Stocke, J.T. & Rector, T.A. 1997 ApJ 489, L17.
- Stickel, M., Fried, J.W. & Kühr, H. 1988 A&A 198, L13.
- Stickel, M., Padovani, P., Urry, C.M., Fried, J.W. & Kühr, H. 1991 ApJ 374, 431.
- Takalo, L. et al. 1998 A&AS 129, 577.
- Urry, C.M. & Padovani, P. 1995 PASP 107, 803.
- Urry, C.M., Falomo, R., Scarpa, R., Pesce, J.E., Treves, A. & Giavalisco, M. 1999 ApJ 512, 88.
- Webb, J.R., Howard, E., Benítez, E., Balonek, T., McGrath, E., Shrader, C., Robson, I. & Jenkins, P. 2000 AJ 120, 41.
- Wurtz, R., Stocke, J.T. & Yee, H.K.C. 1997 ApJ 480, 5.

TABLE 1. GRAVITATIONAL LENS CANDIDATES

Object	z_{em}	z_{abs}	$\log P_{ext}$	f
S5 0454+844	...	1.340	≥ 27.31	> 55.5
PKS 0735+178	...	0.424	≥ 27.30	231
S4 0814+425	> 116.5
PKS 0823+033	0.506:	...	27.31	151.7
PKS 1749+096	0.320:	...	26.59	> 145
S4 1749+701	0.770:	...	27.23	15.8
PKS 2131-021	1.285	...	27.99	6.9

TABLE 2. OBSERVED RADIO PROPERTIES OF THE SAMPLE

Object	4.86 GHz		8.46 GHz		14.94 GHz	
	f_{core} (mJy)	f_{ext} (mJy)	f_{core} (mJy)	f_{ext} (mJy)	f_{core} (mJy)	f_{ext} (mJy)
S5 0454+844	233.3	< 0.5	216.5	< 1.5
PKS 0735+178	975.5	32.2 ± 3.3	838.9	29.3 ± 6.6
S4 0814+425	1011.9	33.0 ± 4.2	1072.3	18.4 ± 6.7
PKS 0823+033	1452.9	< 1.4	1547.6	< 1.8
PKS 1749+096	3794.6	< 2.0	3622.3	< 2.7
S4 1749+701	520.9	31.0 ± 1.1	459.9	18.6 ± 5.8
PKS 2131-021	1732.1	70.8 ± 8.0	1802.0	36.3 ± 6.7

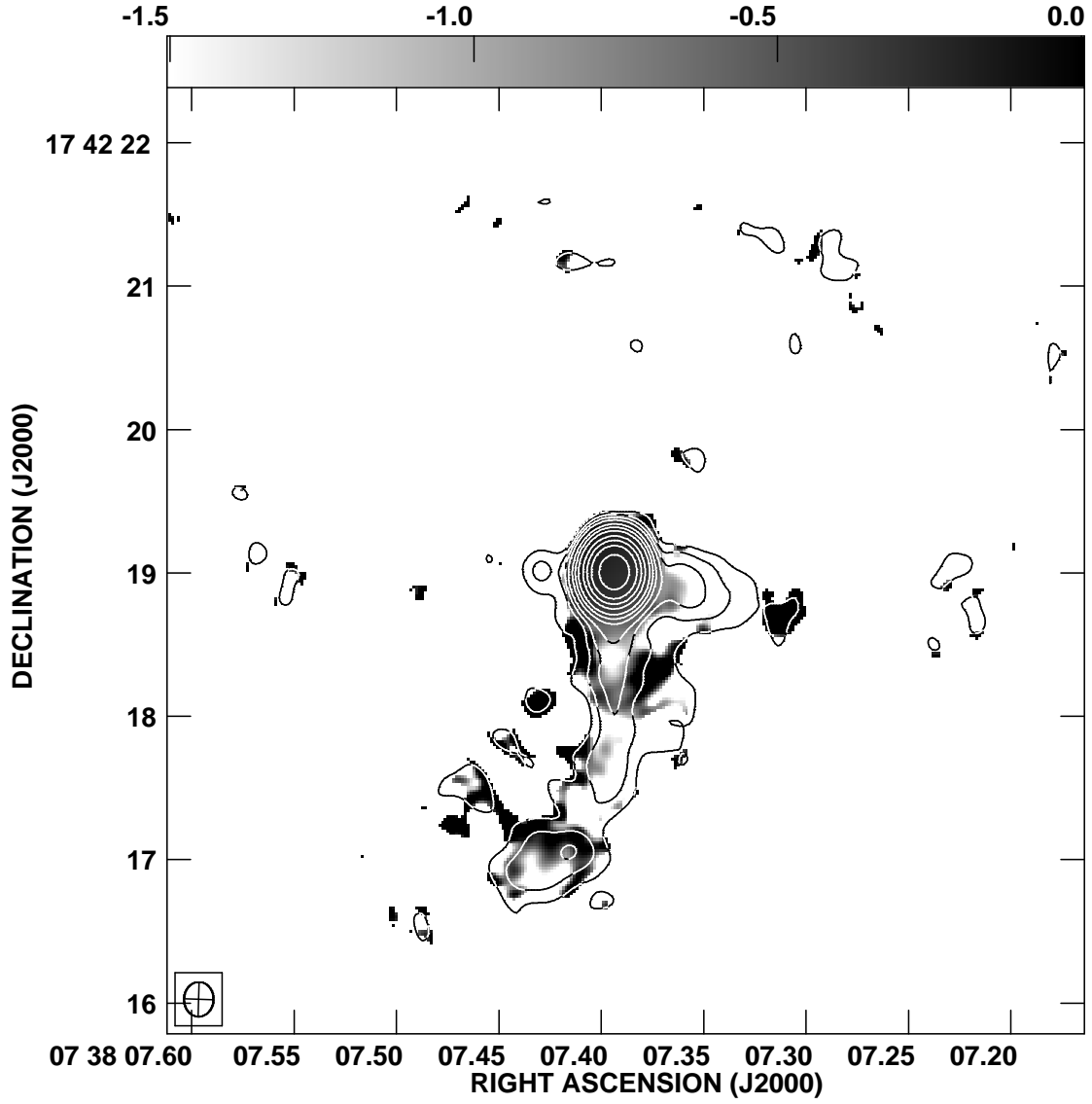


FIG. 1.— VLA 8.46 GHz map (contour) and spectral index map (grayscale) of PKS 0735+178. The beam is shown in the lower left corner. The contour levels are 0.02, 0.05, 0.1, 0.2, 0.5, 1, 2, 5, 10, 20, 50 and 100% the peak flux of 9.755×10^{-1} Jy beam $^{-1}$. The spectral index range is from -1.5 to 0 .

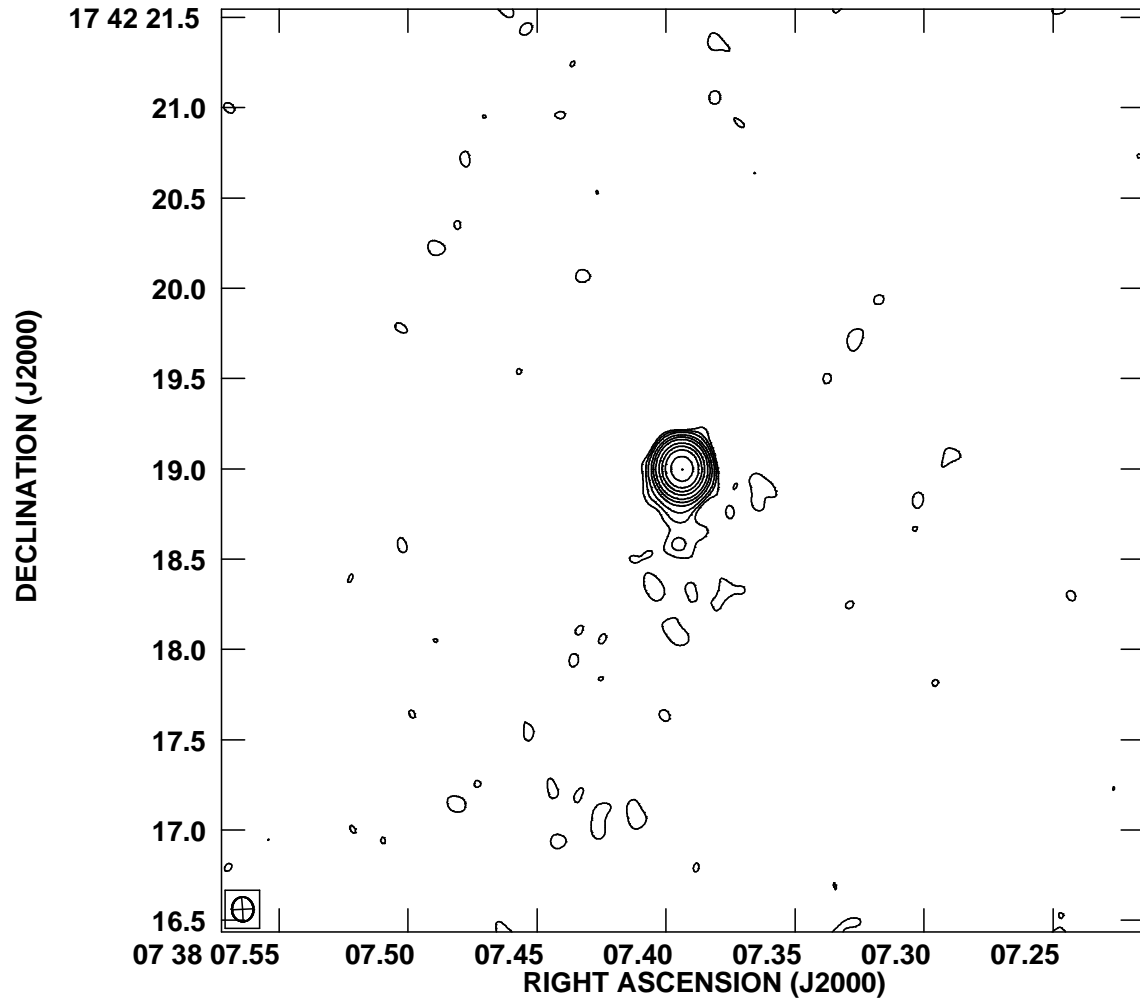


FIG. 2.— VLA 14.94 GHz map of PKS 0735+178. The beam is shown in the lower left corner. The contour levels are 0.05, 0.1, 0.2, 0.5, 1, 2, 5, 10, 20, 50 and 100% the peak flux of $8.389 \times 10^{-1} \text{ Jy beam}^{-1}$.

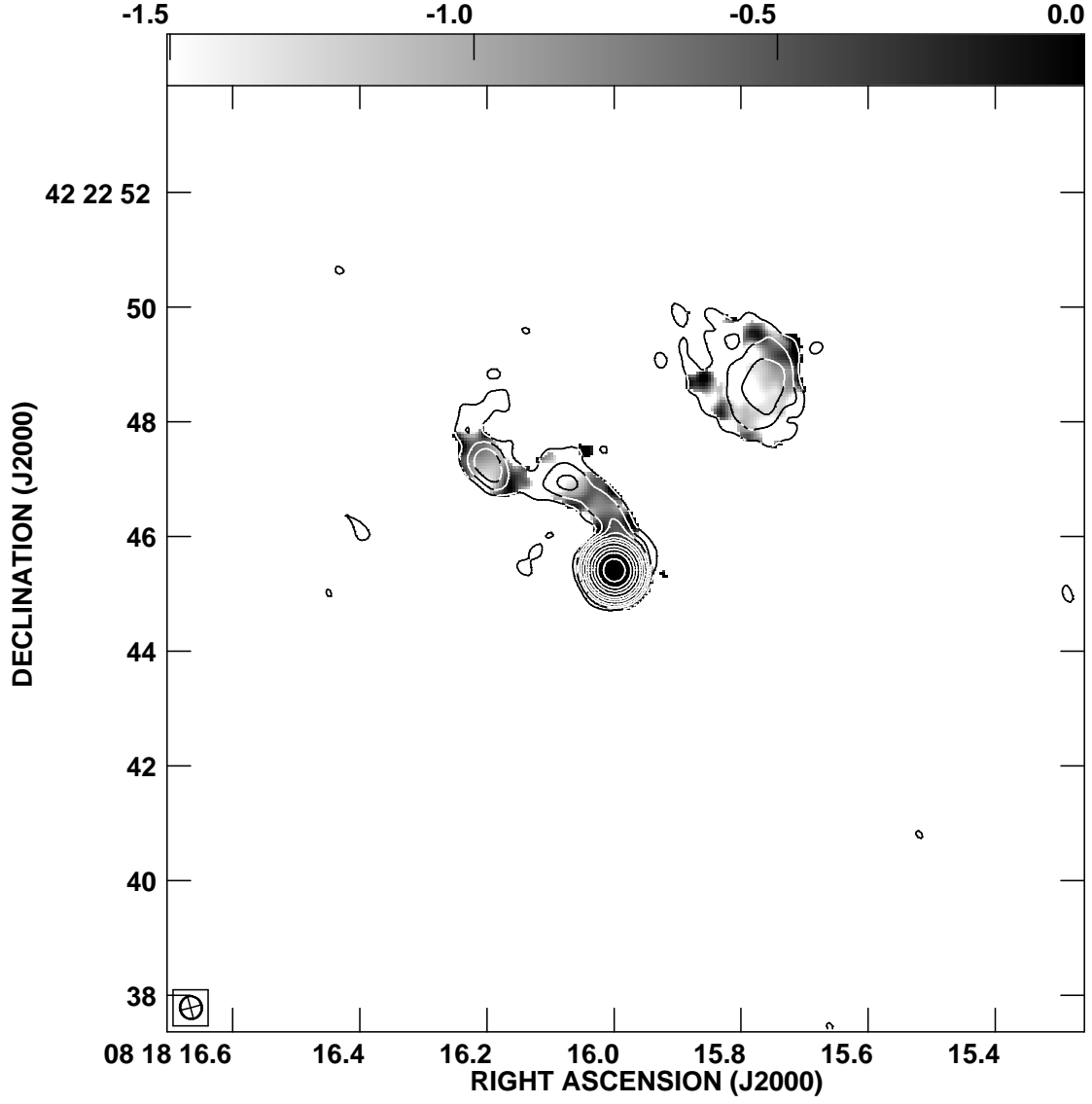


FIG. 3.— VLA 4.86 GHz map (contour) and spectral index map (grayscale) of S4 0814+425. The beam is shown in the lower left corner. The contour levels are 0.02, 0.05, 0.1, 0.2, 0.5, 1, 2, 5, 10, 20, 50 and 100% the peak flux of $1.0119 \text{ Jy beam}^{-1}$. The spectral index range is from -1.5 to 0 .

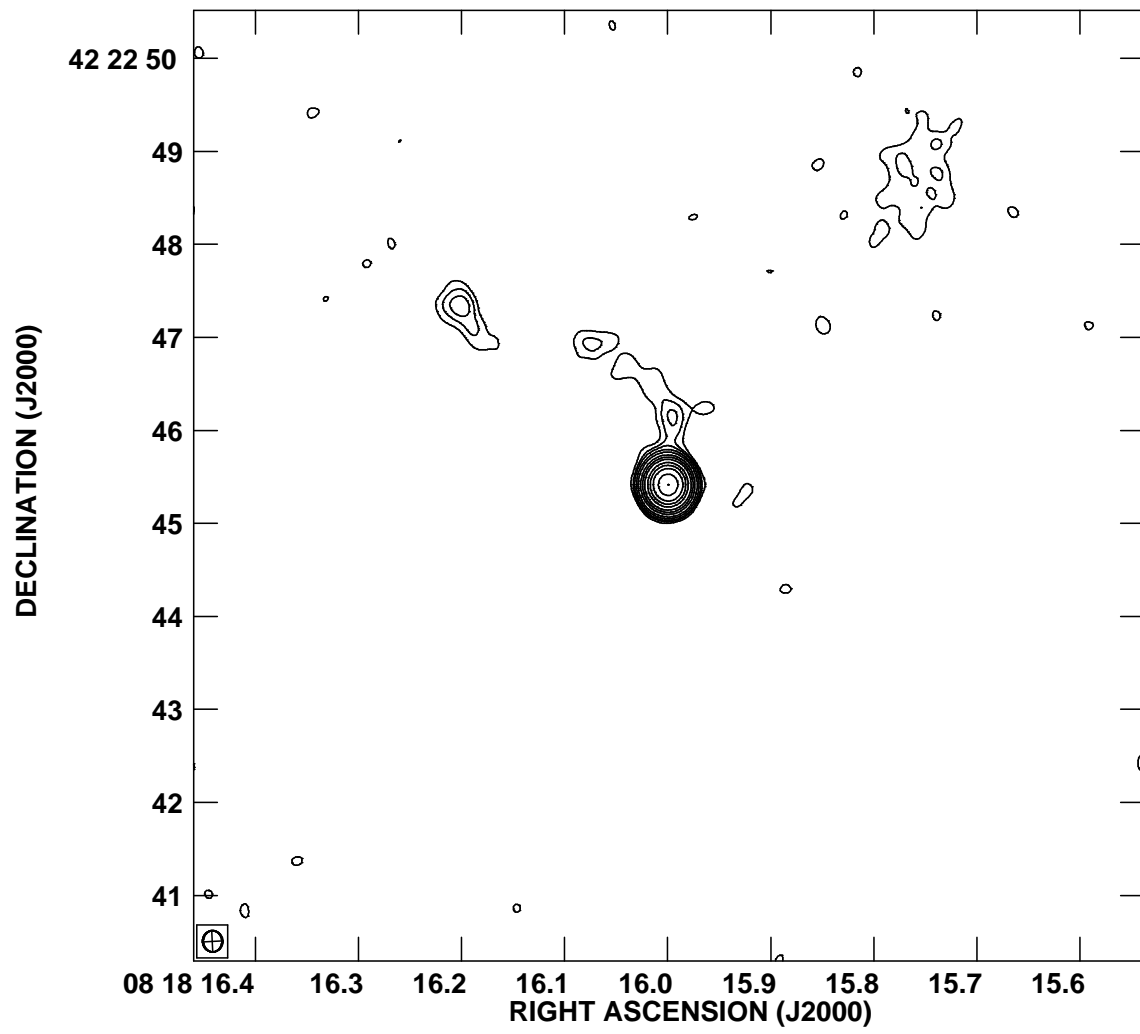


FIG. 4.— VLA 8.46 GHz map of S4 0814+425. The beam is shown in the lower left corner. The contour levels are 0.02, 0.05, 0.1, 0.2, 0.5, 1, 2, 5, 10, 20, 50 and 100% the peak flux of $1.0723 \text{ Jy beam}^{-1}$.

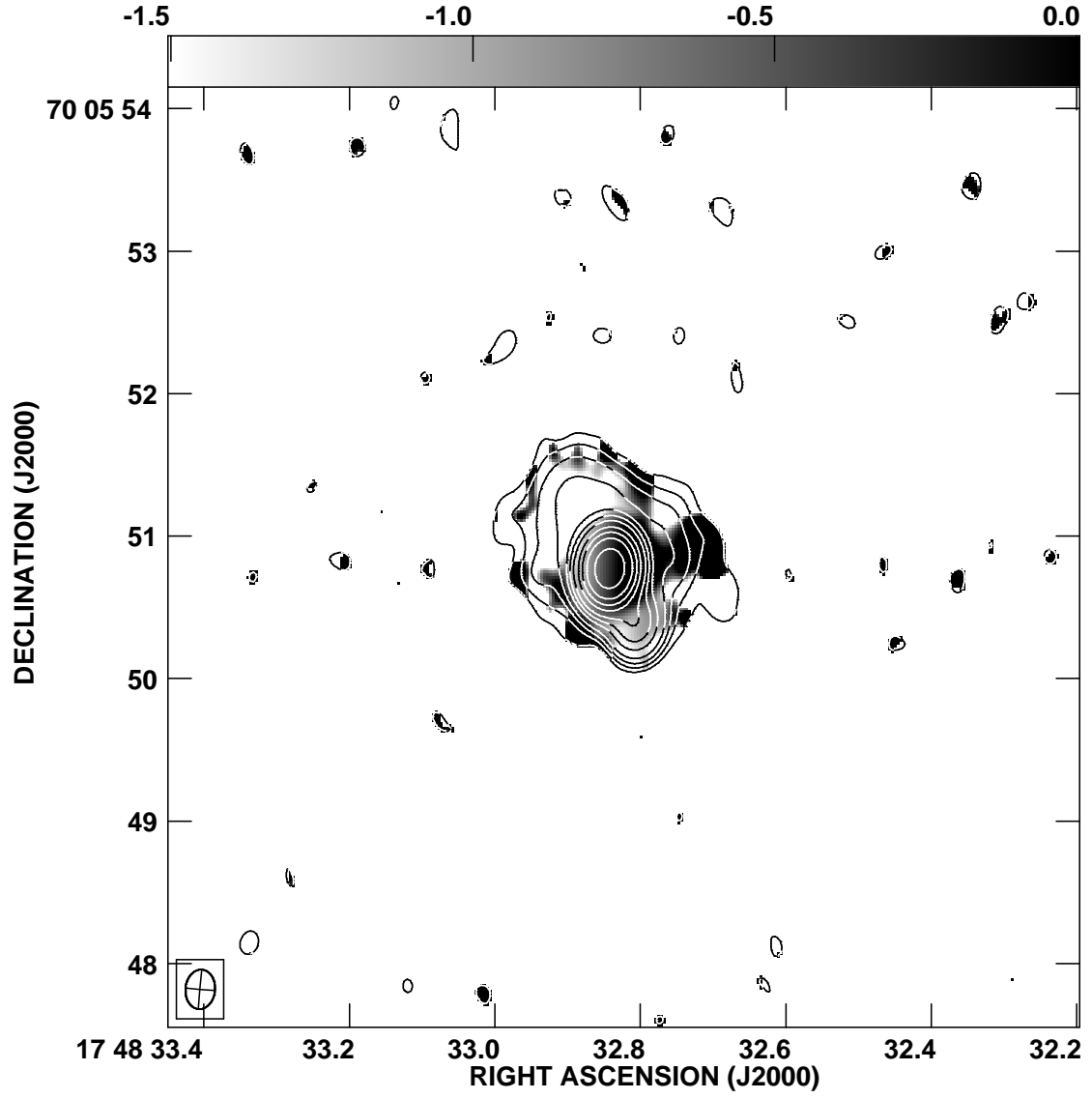


FIG. 5.— VLA 8.46 GHz map (contour) and spectral index map (grayscale) of S4 1749+701. The beam is shown in the lower left corner. The contour levels are 0.02, 0.05, 0.1, 0.2, 0.5, 1, 2, 5, 10, 20, 50 and 100% the peak flux of 5.209×10^{-1} Jy beam $^{-1}$. The spectral index range is from -1.5 to 0 .

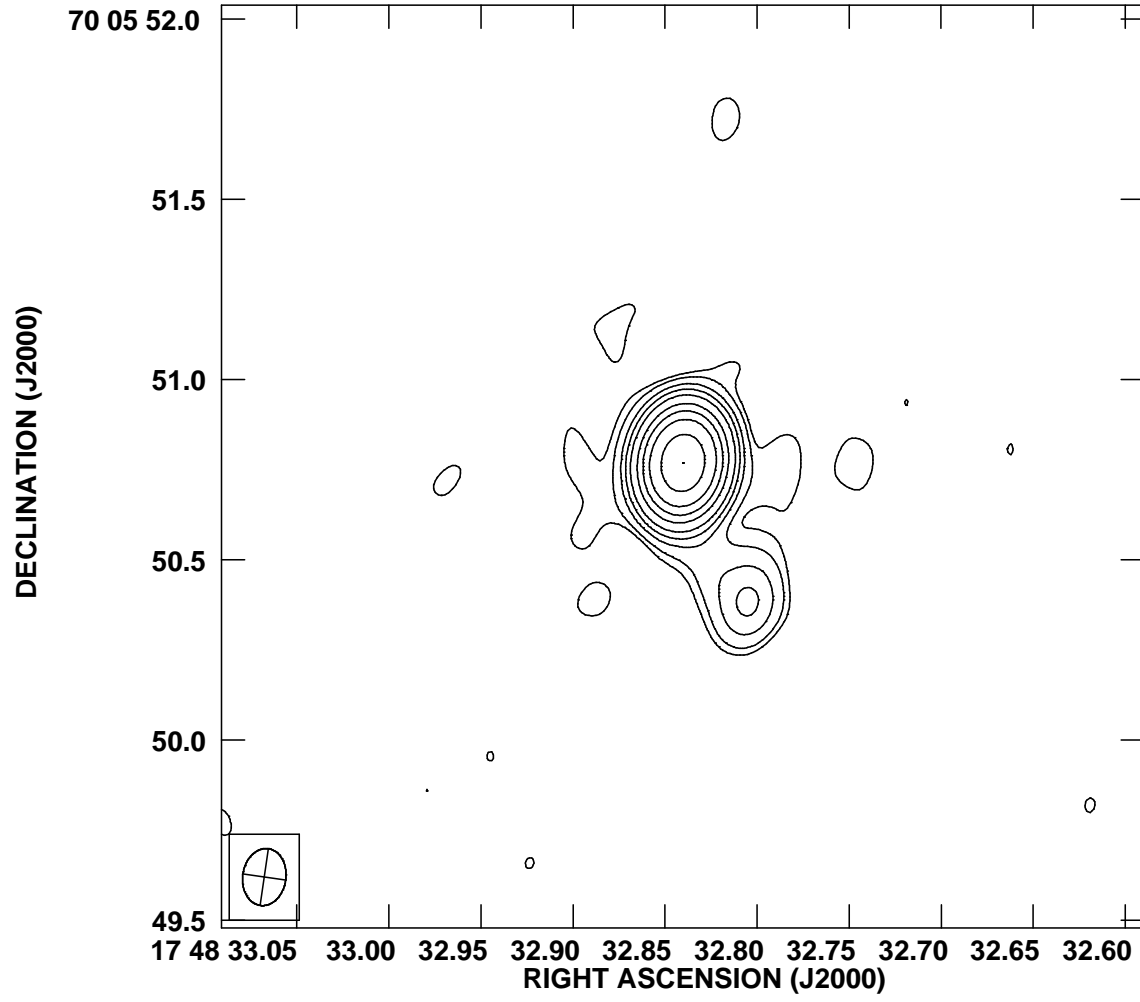


FIG. 6.— VLA 14.94 GHz map of S4 1749+701. The beam is shown in the lower left corner. The contour levels are 0.02, 0.05, 0.1, 0.2, 0.5, 1, 2, 5, 10, 20, 50 and 100% the peak flux of $4.599 \times 10^{-1} \text{ Jy beam}^{-1}$.

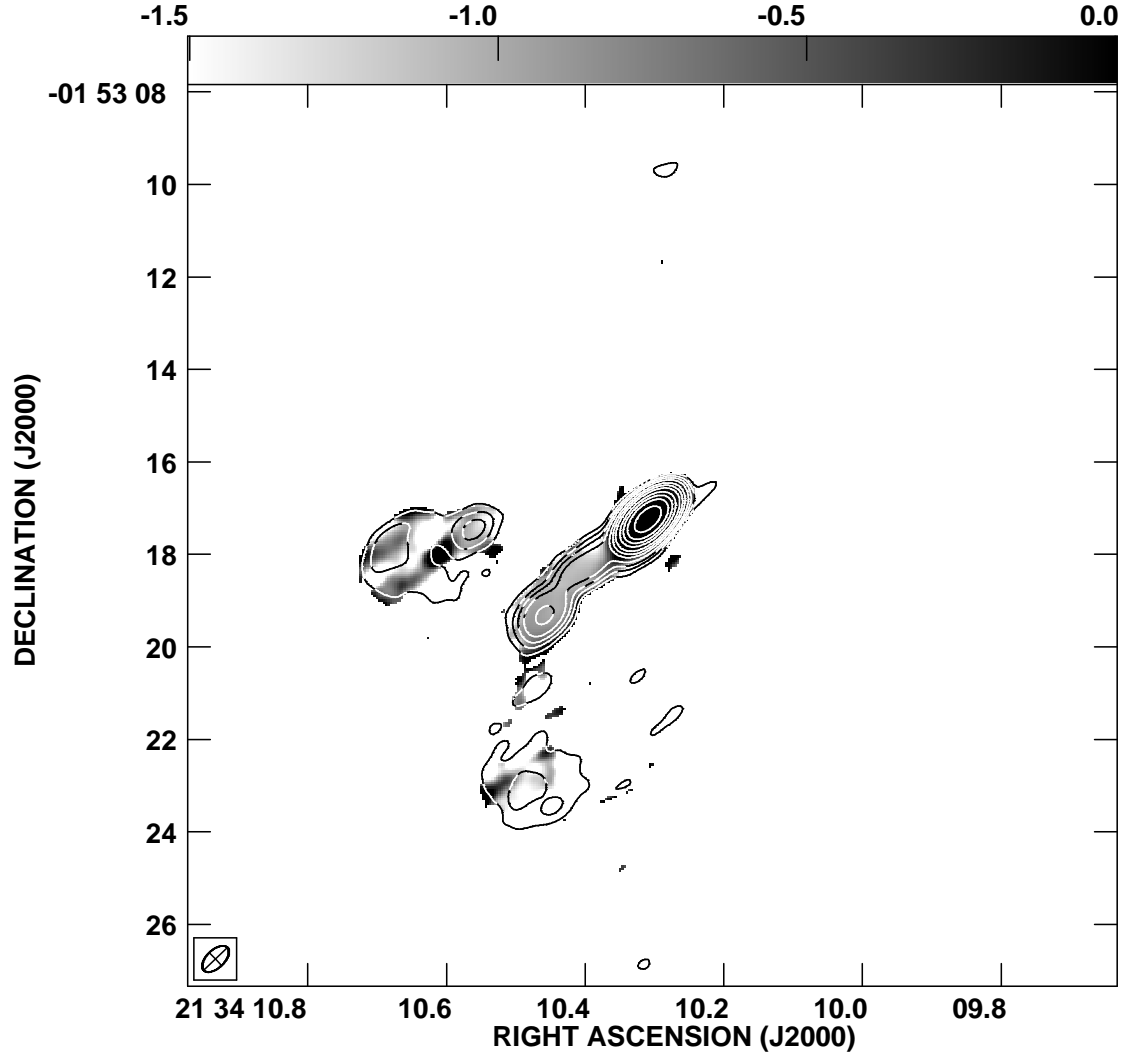


FIG. 7.— VLA 4.86 GHz map (contour) and spectral index map (grayscale) of PKS 2131-021. The beam is shown in the lower left corner. The contour levels are 0.02, 0.05, 0.1, 0.2, 0.5, 1, 2, 5, 10, 20, 50 and 100% the peak flux of 1.7321 Jy beam⁻¹. The spectral index range is from -1.5 to 0.

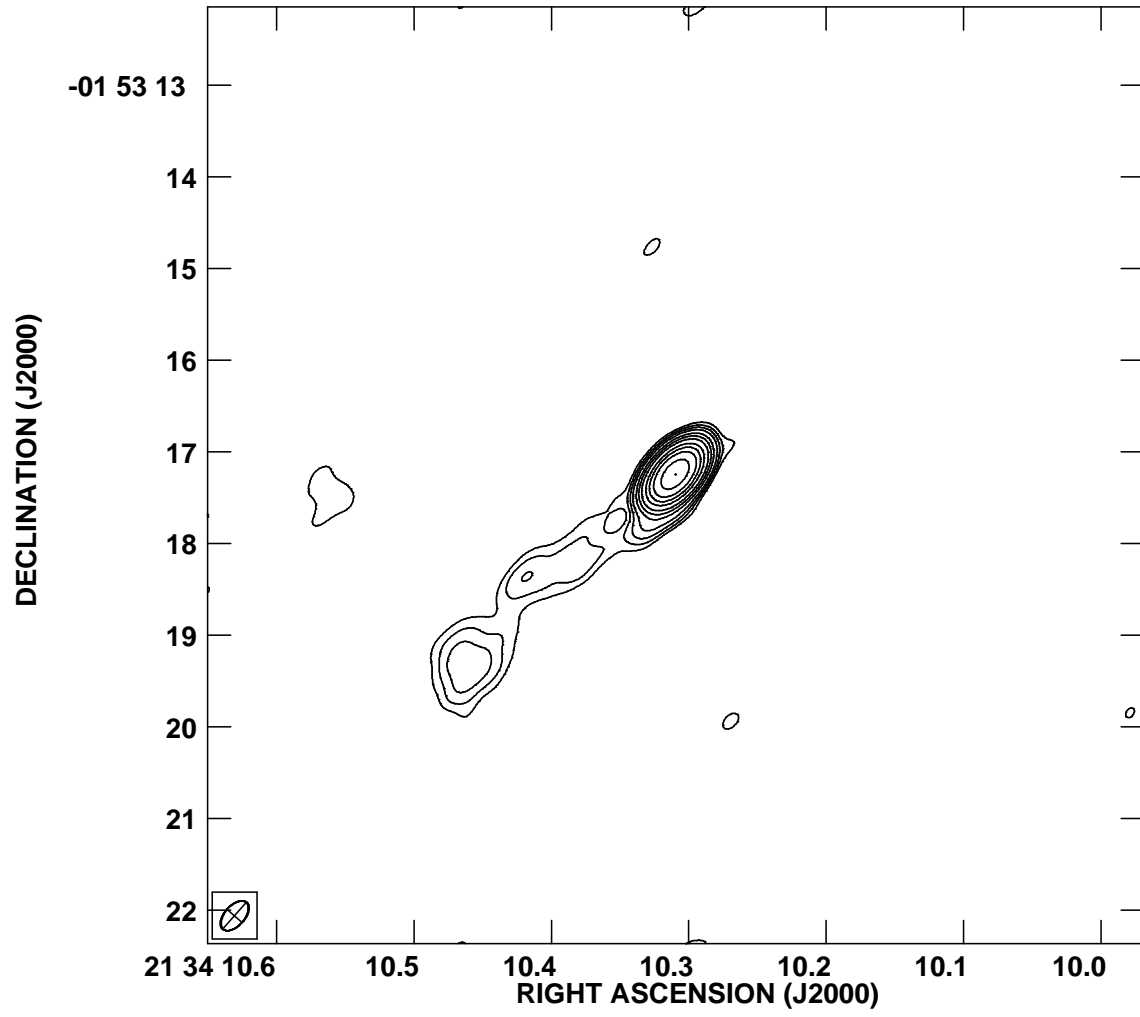


FIG. 8.— VLA 8.46 GHz map of PKS 2131–021. The beam is shown in the lower left corner. The contour levels are 0.02, 0.05, 0.1, 0.2, 0.5, 1, 2, 5, 10, 20, 50 and 100% the peak flux of $1.8020 \text{ Jy beam}^{-1}$.